energies

MDPI

Article

A Novel Denoising Method for Partial Discharge Signal Based on Improved Variational Mode Decomposition

Jingjie Yang [1], Ke Yan [2], Zhuo Wang [1] and Xiang Zheng [1,*]

[1] School of Automation and Electrical Engineering, Dalian Jiaotong University, Dalian 116028, China
[2] Co-Innovation Center for Sustainable Forestry in Southern China, College of Biology and the Environment, Nanjing Forestry University, Nanjing 210037, China
* Correspondence: zxyh2001@163.com

Abstract: Partial discharge (PD) online monitoring is a common technique for high-voltage equipment diagnosis. However, due to field interference, the monitored PD signal contains a lot of noise. Therefore, this paper proposes a novel method by integrating the flower pollination algorithm, variational mode decomposition, and Savitzky–Golay filter (FPA-VMD-SG) to effectively suppress white noise and narrowband noise in the PD signal. Firstly, based on the mean envelope entropy (MEE), the decomposition number and quadratic penalty term of the VMD were optimized by the FPA. The PD signal containing noise was broken down into intrinsic mode functions (IMFs) by optimized parameters. Secondly, the IMFs were classified as the signal component, the noise dominant component, and the noise component according to the kurtosis value. Thirdly, the noise dominant component was denoised using the SG filter, and the denoised signal was mixed with the signal component to reconstruct a new signal. Finally, threshold denoising was used to eliminate residual white noise. To verify the performance of the FPA-VMD-SG method, compared with empirical mode decomposition with wavelet transform (EMD-WT) and adaptive singular value decomposition (ASVD), the denoising results of simulated and real PD signals indicated that the FPA-VMD-SG method had excellent performance.

Keywords: variational mode decomposition; flower pollination algorithm; SG filter; mean envelope entropy; denoising; partial discharge

Citation: Yang, J.; Yan, K.; Wang, Z.; Zheng, X. A Novel Denoising Method for Partial Discharge Signal Based on Improved Variational Mode Decomposition. *Energies* **2022**, *15*, 8167. https://doi.org/10.3390/en15218167

Academic Editor: Hazlee Azil Bin Illias

Received: 28 September 2022
Accepted: 31 October 2022
Published: 2 November 2022

1. Introduction

A healthy insulation condition is the premise for ensuring the stable running of power equipment [1]. Partial discharge (PD) is one of the primary features that can effectively reflect the internal insulation defects of power equipment [2]. Online PD measurement has been particularly developed and widely used because of its high sensitivity and accuracy of insulation conditions [3]. However, field noise, which includes white noise, periodic narrowband interference, and pulse interference, can influence the detection and identification of the PD signal. Effectively suppressing field noise interference is an essential issue for monitoring the insulation conditions of power equipment [4]. White noise that conforms to the Gaussian distribution produces erratic interference from the field erratic interference. The principal sources of periodic narrowband interference are high-order harmonics, radio transmissions, and broadcast signals. Pulse interference is produced by switching the operation of thyristors and other equipment. The high strength and low frequency of pulse interference make it simple to eliminate. Therefore, eliminating white noise and narrowband noise is critical for PD signal extraction and analysis [5].

Over the past few years, researchers have proposed several algorithms for PD signal denoising, such as the wavelet transform (WT) [6,7], the empirical modal decomposition (EMD) [8] and its improvements, [9,10], the singular value decomposition (SVD) [11,12], and the variational mode decomposition (VMD) [13,14]. The WT has a great time-frequency

analysis capability, but its signal decomposition depends on the wavelet type and order, the decomposition degree, and the threshold type. EMD has excellent stability for adaptively breaking down the signal into different modal components. However, modal mixing is more likely to happen when the frequency of each component is close together. To solve the modal mixing phenomenon in the EMD method, research based on EMD proposed ensemble empirical mode decomposition (EEMD) [15], complete ensemble empirical mode decomposition (CEEMD) [16], and complete ensemble empirical mode decomposition with adaptive noise (CEEMDAN) [17]. Unfortunately, the problem of modal mixing was not completely solved. SVD can be applied to rebuild and eliminate narrowband noise in the PD signal noise [18], but the singular values between the PD signal and white noise are difficult to distinguish. SVD is thus unsuitable for eliminating white noise [11].

VMD, a novel signal analysis method, was proposed by Dragomiretskiy and Zosso in 2014 [19]. This method overcomes various problems in current signal decomposition technology, such as modal mixing and the endpoint effect. However, the parameters of VMD, including the decomposition number, quadratic penalty term, and time step, need to be artificially set. When the parameter setting is unreasonable, the ideal results cannot be obtained. Therefore, the parameters of VMD need to be adaptively optimized to obtain better decomposition results. Some researchers adjusted the decomposition number using EMD [13] and optimized the time step using the particle swarm optimization (PSO) algorithm [14]. None of these studies attempted to consider the quadratic penalty term. Moreover, the PSO algorithm converges quickly, but easily falls into the local optimum. Now, many nature-inspired optimization algorithms have been proposed. The flower pollination algorithm (FPA) has been widely used because it has few parameters and is easily adjusted [20]. The verification shows that the algorithm has high efficiency and an almost exponential convergence speed [21].

At present, VMD optimization mainly takes the minimum energy loss and highest kurtosis value as the objective function [14]. Envelope entropy can reflect the magnitude of signal fluctuation and can also be used as an objective function for optimizing VMD, which has been verified in the field of rolling bearing [22]. The intrinsic mode functions (IMFs) generated by VMD decomposition still need to be classified and denoised. The Savitzky–Golay (SG) filter can remove noise by smoothing data without changing the trend in the data [23], but it has not been applied in the realm of PD denoising.

Therefore, this paper proposes the FPA-VMD-SG method as a solution to the aforementioned issues. Taking the mean envelope entropy (MEE) as the objective function adaptively optimizes the decomposition number and quadratic penalty term of VMD. The IMFs decomposed by VMD were divided into three categories: signal component, noise dominant component, and noise component. The dominant noise component was denoised using an SG filter, and the denoised signal was mixed with the signal component to reconstruct a new signal. Eliminating residual white noise in the new signal used threshold denoising to obtain the final denoised PD signal. A comparative analysis with empirical mode decomposition with wavelet transform (EMD-WT) and adaptive singular value decomposition (ASVD) was performed using simulated and real PD signals. The performance metrics of three methods were calculated to verify the performance of the FPA-VMD-SG method.

2. Basic Theory

2.1. Variational Mode Decomposition

VMD that can disintegrate a complex discrete signal into simple modal components, and is a completely non-recursive signal decomposition method [19]. The specific steps are as follows:

Step1: The variational problem is that the sum of the estimated bandwidth of the IMFs is the smallest. The limitation condition is that the sum of the IMFs is the original signal. The formula is as follows:

$$\begin{gathered}\min_{\{u_k,\ \omega_k\}}\left\{\sum_k \left\|\partial_t\left[\left(\delta(t)+\frac{j}{\pi t}\right)*u_k(t)\right]e^{-j\omega_k t}\right\|_2^2\right\} \\ s.t.\ \ f(t)=\sum_{k=1}^{K}u_k(t)\end{gathered} \tag{1}$$

where $\{u_k\}$ is the set of IMFs, $\{\omega_k\}$ is the set of central frequencies, $\delta(t)$ is the impulse function, K is the preset decomposition number, and $f(t)$ is the original function.

Step2: The quadratic penalty term α and the Lagrange multiplier $\lambda(t)$ are used to convert the constrained variational problem into the unconstrained problem. The α affects the reconstruction accuracy of the signal and the $\lambda(t)$ maintains the strictness of the constraint condition. The formula is as follows:

$$\begin{aligned}L(\{u_k\},\{\omega_k\},\lambda)=\alpha\sum_k\left\|\partial_t\left[\left(\delta(t)+\frac{j}{\pi t}\right)*u_k(t)\right]e^{-j\omega_k t}\right\|_2^2 \\ +\left\|f(t)-\sum_{k=1}^{K}u_k(t)\right\|_2^2+\left\langle\lambda(t),f(t)-\sum_{k=1}^{K}u_k(t)\right\rangle\end{aligned} \tag{2}$$

Step3: The unconstrained problem is solved by the alternating direction multiplier method, so as to realize the effective separation of the signal frequency. The iterative updating and center frequency of the IMF are as follows:

$$\hat{u}_k^{n+1}=\frac{\hat{f}(\omega)-\sum_{i\neq k}\hat{u}_i(\omega)+\frac{\hat{\lambda}(\omega)}{2}}{1+2\alpha(\omega-\omega_k)^2} \tag{3}$$

$$\omega_k^{n+1}=\frac{\int_0^\infty\omega|\hat{u}_k(\omega)|^2d\omega}{\int_0^\infty|\hat{u}_k(\omega)|^2d\omega} \tag{4}$$

where $\hat{u}_k^{n+1}$ is the kth IMF with center frequency ω at the (n+1)th iteration. The inverse Fourier transform is performed on $\hat{u}_k(\omega)$, and the actual part $u_k(t)$. ω_k^{n+1} is the center frequency of the kth IMF at the (n+1)th iteration.

2.2. Flower Pollination Algorithms

The FPA was developed by Xin-She Yang in 2012, and inspired by the pollination process of flowering plants [21]. The FPA was iterated by self-pollination and cross-pollination. This algorithm was a fashionable intelligent optimization algorithm with the advantages of fast speed and not being easy to fall into local extremum. The specific steps are as follows:

Step1: Input the maximum number of iterations, population individual number, flower individual interval, conversion probability, and other algorithm parameters.

Step2: Set the decomposition number K as an integer from 2 to 11, and set the quadratic penalty term α as the search variable with a range from 100 to 10,000.

Step3: Create the initial population randomly with uniform distribution, and calculate the fitness value. Then, retain the global optimal individual and the optimal fitness under the current population. Fitness is the objective function.

Step4: Create a stochastic number ε randomly with uniform distribution. If the random number is less than the conversion probability, a new individual is created by cross-pollination, as shown in (5). Conversely, a new individual is produced by self-pollination, as shown in (6):

$$x_i^{t+1}=x_i^t+\gamma L\left(x_i^t-g_*\right) \tag{5}$$

$$x_i^{t+1}=x_i^t+\varepsilon\left(x_j^t-x_k^t\right) \tag{6}$$

where x_i^t is the pollen i at iteration t, and x_j^t and x_k^t are pollens from the different flowers of the same plant species, g_* is the current best solution found among all solutions in the current iteration, γ is a scaling factor for controlling step length, and L is the strength of the pollination.

Step5: Replace all individuals in the population with new individuals to produce new populations.

Step6: Check the interval of new populations. The individual exceeding the interval maximum value is set to the maximum value of the interval, and the individual below the minimum value of the interval is set to the minimum value of the interval.

Step7: Calculate the fitness value of the new population, and update the global optimal individual and the optimal fitness.

Step8: Determine whether the maximum number of iterations is reached. If not, repeat Step4 to Step7. Otherwise output the global optimal individual and the optimal fitness.

2.3. Envelope Entropy

The envelope entropy reflects the magnitude of signal envelope fluctuation. The following is a definition of envelope entropy [22]:

$$\begin{aligned} E_c &= -\sum_{i=1}^{N} c_i lg(c_i) \\ c_i &= a(i) / \sum_{i=1}^{N} a(i) \end{aligned} \tag{7}$$

where $a(i)$ is obtained by Hilbert transform of a signal $x(t)$ with length N, and c_i is the regularization result of $a(i)$.

MEE is selected as the objective function in this paper and expressed in the following formula:

$$MEE = \frac{1}{m} \sum_{i=1}^{m} E_{ci} \tag{8}$$

where m is the number of IMFs generated by the VMD. The smaller the MME, the lower the complexity of the corresponding IMFs.

2.4. Kurtosis

Kurtosis is a characteristic parameter used to measure the outlier degree of outlier data. PD signal is a kind of short-term and abrupt pulse signal, and its kurtosis value is large. The kurtosis value of the signal without PD is about 3. When PD occurs, the kurtosis value is much larger than 3 [5]. The kurtosis value is defined as:

$$Ku = \frac{E\left[(x-\mu)^4\right]}{\left(E\left[(x-\mu)^2\right]\right)^2} \tag{9}$$

where μ is the mean value of the signal, and x represents a set of outlier data.

2.5. Savitzky–Golay Filter

Savitzky and Golay proposed a method for smoothing and differentiating noisy discrete data based on local least squares polynomial approximation [24]. The SG filter that can be used to smooth a set of data is a digital filter. It can increase the accuracy of the data without changing the trend and width of the signal, indicating that this method has excellent results in dealing with nonlinear and aperiodic signals. The smoothing steps of the SG filter are as follows [25]:

Step1: Input a set of data $\{x_k\}$.

Step2: Construct a n-order polynomial to fit data $\{x_k\}$, and the fitted equation is expressed in the following formula:

$$p(k) = \sum_{i=0}^{n} b_i k^i \tag{10}$$

where $p(k)$ is the fitted value, n is the order of polynomial, and b_i is the coefficient of k^i.

Step3: Calculate the quadratic sum of the residuals value between fitting data points and original data points. It is defined as:

$$\delta = \sum_{k=-m}^{m} (p(k) - x_k)^2 \tag{11}$$

where δ is the residual value.

Step4: Perform the smoothing process in a sliding window until all values are smoothed.

2.6. Threshold Denoising

Threshold denoising can suppress useless noise in the signal and retain the useful signal. According to the distribution characteristics of white noise, threshold denoising based on the 3σ rule is introduced [5]. The formula is as follows:

$$th = c \cdot 3\sigma \tag{12}$$

$$y(i) = \begin{cases} p(i), & |p(i)| \geq th \\ 0, & |p(i)| < th \end{cases}, \quad i = 1, 2, \cdots, N \tag{13}$$

where c is a coefficient and σ is the standard deviation of p. The denoising effect can be improved by adjusting the threshold of c.

3. Denoising Method

3.1. Simulated PD Signal

The simulated PD signal can be simulated by single exponential decaying oscillation and double exponential decaying oscillation. The calculation formulas of these two mathematical models are as follows [12]:

$$x_1(t) = A_1 \cdot e^{-t/\tau} \cdot \sin(2\pi f_c t) \tag{14}$$

$$x_2(t) = A_2 \cdot \left(e^{-1.3t/\tau} - e^{-2.2t/\tau}\right) \cdot \sin(2\pi f_c t) \tag{15}$$

where A_1 and A_2 are the amplitude of the PD signal, τ is the decaying coefficient, and f_c is the oscillation frequency. The detailed parameters of the four PD pulses are shown in Table 1. The PD pulse s_1 and s_2 are calculated by (14), and s_3 and s_4 are calculated by (15). The simulated sampling frequency is 1GHz. The original PD signal and its frequency spectrum are shown in Figure 1.

Table 1. The PD simulation model parameters.

PD Pulse	τ/ns	f_c/MHz	A/mv
s_1	10	100	0.5
s_2	10	100	0.5
s_3	10	100	2
s_4	10	100	2

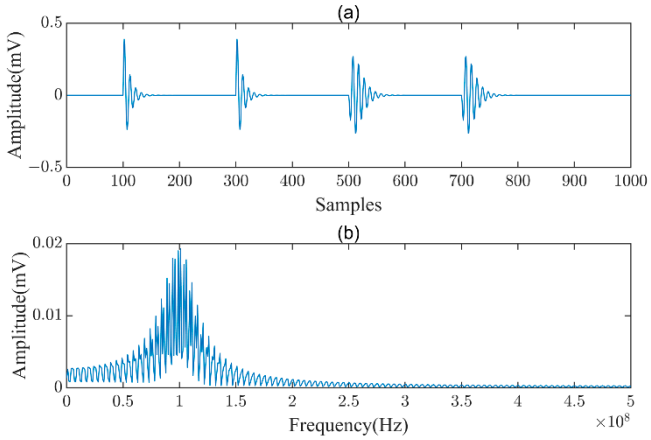

Figure 1. Simulated the original signal: (**a**) original PD signal; (**b**) frequency spectra.

Then, white noise and narrowband noise are mixed with the original signal to obtain the noisy PD signal. The white noise is generated by Gaussian white noise simulation. The mathematical formula for narrowband noise is shown in (16). The noisy PD signal and its frequency spectrum are shown in Figure 2:

$$S = A * \sum_{i=1}^{3} \sin(2\pi f_i t) \tag{16}$$

where the amplitude A is set to 0.2 mV, and the narrowband noise frequency f_i is set to $f_1 = 50$ MHz, $f_2 = 90$ MHz, and $f_3 = 150$ MHz [5]. As observed in Figure 2a, the original signal is completely covered by the noisy signal.

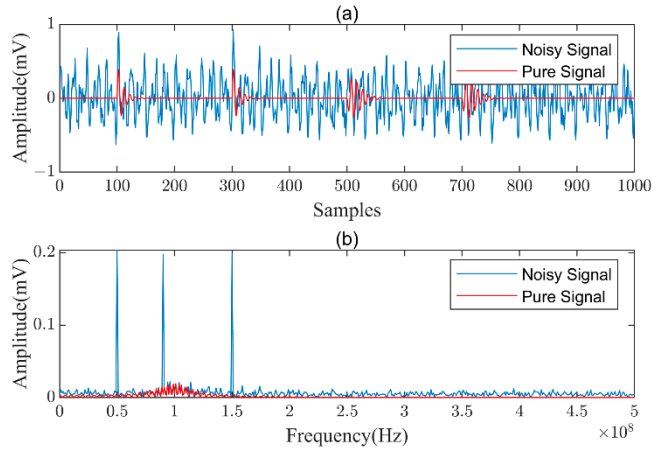

Figure 2. Simulated the noisy signal: (**a**) noisy PD signal; (**b**) frequency spectra.

3.2. Proposed FPA-VMD-SG Denoising Method

Figure 3 outlines the approach followed in the proposed FPA-VMD-SG denoising method. The steps of the method are as follows:

Step1: Optimize the parameters of the VMD using the FPA, with the MME as an objective function.

Step2: Calculate the kurtosis value for each IMF of the VMD.

Step3: Divide the IMFs into the signal component, the noise dominant component, and the noise component, according to the kurtosis value and frequency spectra of each IMF.

Step4: Denoise the noise dominant component with the SG filter and discard the noise component.

Step5: Mix the denoised signal and the signal component to reconstruct the signal.

Step6: Remove residual white noise using threshold denoising to obtain the denoised PD signal.

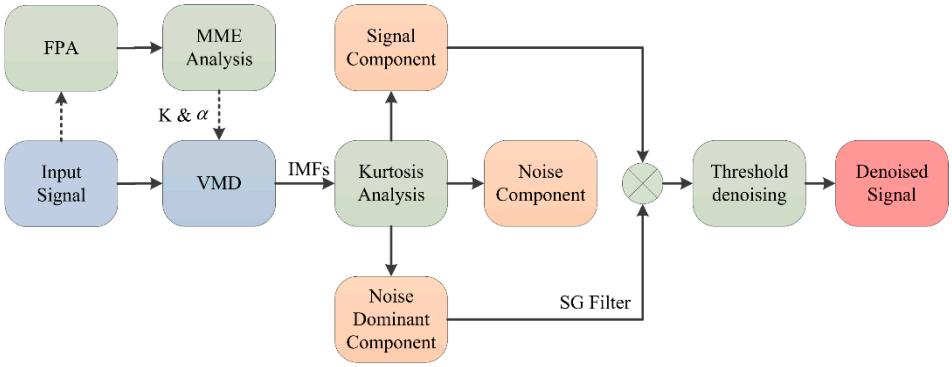

Figure 3. Overall process flow diagram of the proposed FPA-VMD-SG denoising method.

3.3. Simulated PD Signal Denoising

When VMD decomposes the signal, the decomposition number depends on the value of K. The signal can be better decomposed when K has a reasonable value. The quadratic penalty term α affects the VMD process to ensure signal reconstruction accuracy.

In this paper, the parameters of FPA are as follows: the number of individuals is 20, the maximum number of iterations is 500, and the conversion probability is 0.5 [21]. The final optimization results are $K = 7$ and $\alpha = 7932.3488$.

Applying the optimized parameters to the VMD parameter settings, the decomposition results are shown in Figure 4. The IMF transition was smooth in the time domain diagram, and different central frequencies were obviously separated in the frequency domain diagram. The central frequencies of IMF2, IM3, and IMF5 were 49.8 MHz, 90.1 MHz, and 150 MHz, respectively. Moreover, their amplitudes were close to 0.2 mV. These three IMFs are similar to narrowband noise. The frequency range of IMF4 was concentrated in the range of the signal component. As concluded from Figures 4 and 5, IMF2, IMF3, and IMF5 were noise components. IMF4 was a signal component. IMF1, IMF6, and IMF7 were noise-dominant components.

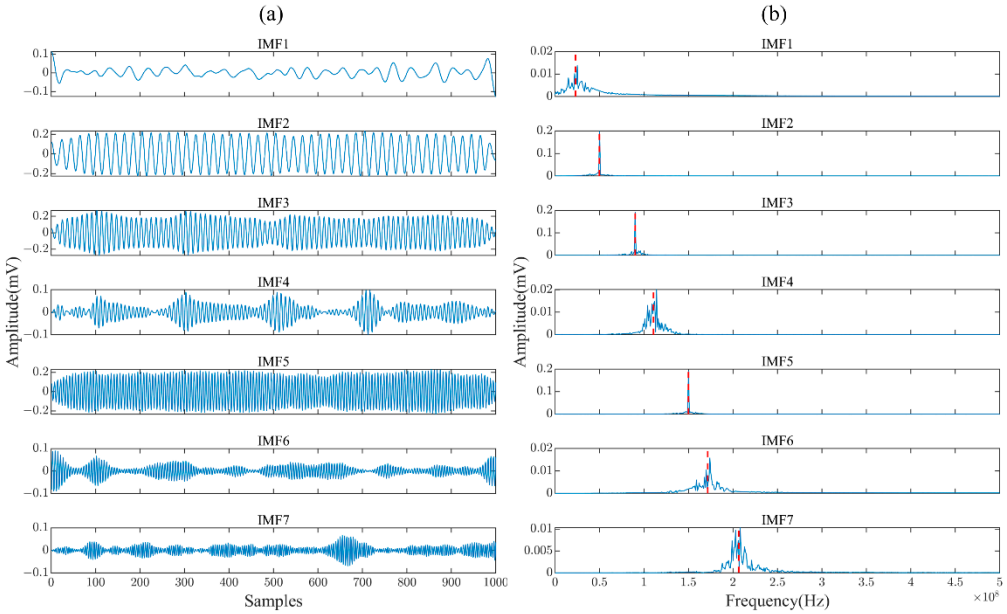

Figure 4. Simulated PD signal decomposition: (**a**) IMFs; (**b**) frequency spectra.

Therefore, it is necessary to use an SG filter that specifies the polynomial order as 4 and frame length as 201 to denoise IMF1, IMF6, and IMF7. The denoised signals were then mixed with IMF4, but a little white noise remained in the newly acquired signal. Thus, threshold denoising was performed on newly acquired signals. The σ in the (12) is

the standard deviation of the IMF4, and c was set to 0.6. After threshold denoising, the denoised signal was finally obtained as shown in Figure 6. The number and characteristics of the PD signal were restored.

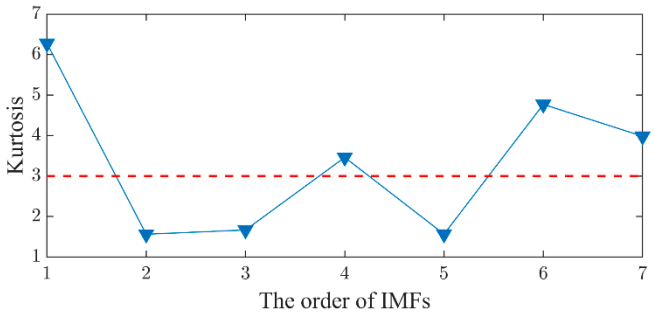

Figure 5. Kurtosis value of each IMF.

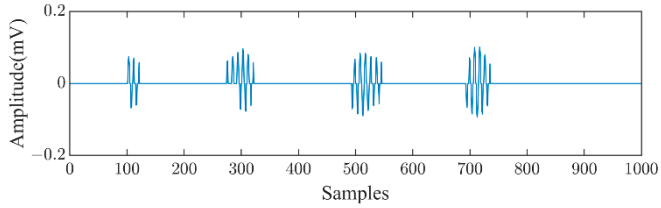

Figure 6. Denoised signal.

4. Comparison and Analysis of Denoising

4.1. Denoising Results of Simulated PD Signal

The simulated PD signal adopted the proposed FPA-VMD-SG method, EMD-WT [26], and ASVD [18] to denoise. EMD-WT can remove most noise, but it also has the disadvantage of removing PD signals (Figure 7b). ASVD can retain the PD signal, but there is still some slight noise (Figure 7c). Compared with EMD-WT and ASVD, the proposed FPA-VMD-SG method performed exceptionally well in removing noise and preserving features, which was conducive to further analysis of the PD signal (Figure 7a).

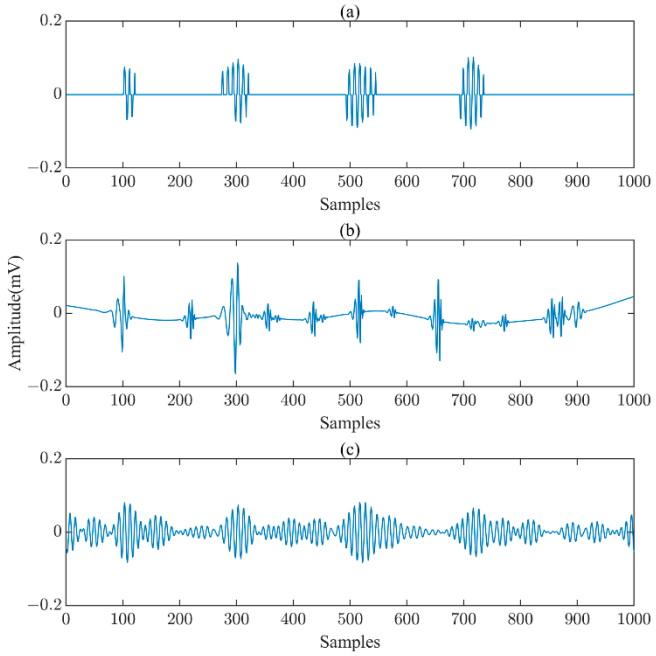

Figure 7. The denoising results of PD signals by different methods: (**a**) FPA-VMD-SG; (**b**) EMD-WT; (**c**) ASVD.

To evaluate and demonstrate the performance of the proposed FPA-VMD-SG method, the following indicators, *SNR* (signal to noise ratio), *NCC* (normalized correlation coefficient), and *RMSE* (root mean squared error) were calculated [5]:

$$SNR = 10 * \log_{10} \frac{\sum_{i=1}^{N} s(i)^2}{\sum_{i=1}^{N} [d(i) - s(i)]^2} \tag{17}$$

$$NCC = \frac{\sum_{i=1}^{N} s(i) * d(i)}{\sqrt{\left(\sum_{i=1}^{N} s(i)^2\right) * \left(\sum_{i=1}^{N} d(i)^2\right)}} \tag{18}$$

$$RMSE = \sqrt{\frac{1}{N} \sum_{i=1}^{N} [d(i) - s(i)]^2} \tag{19}$$

where s is the original PD signal, d is the denoised PD signal, and N is the length of the signal.

The *SNR* was used to evaluate the denoising performance. The *NCC* was used to evaluate the waveform similarity between the denoised signal and original signal. The *RMSE* was used to evaluate waveform distortion of the denoised signal relative to the original signal. The *SNR* value was higher, the *NCC* value was closer to 1 [27], and the *RMSE* value was lower, indicating that the denoising performance was better.

The indicator values of the three denoising methods are shown in Table 2. The FPA-VMD-SG method had higher *SNR*, higher *NCC*, and lower *RMSE*, showing that it had better denoising performance than other methods.

Table 2. Indicator values of three denoising methods.

	SNR	***NCC***	***RMSE***
EMD-WT	5.8567	0.2310	0.520
ASVD	5.9344	0.6007	0.0413
FPA-VMD-SG	8.1584	0.7020	0.0399

4.2. Denoising Results of Real PD Signal

The void discharge signal, as the real PD signal, was available in [28] to validate the quality of the proposed method. Figure 8 shows that the real PD signal was not interfered with by narrowband noise. Therefore, the real PD signal was considered to have mixed two narrowband noises with amplitudes of 0.5 mV. The frequencies of the two narrowband noises were 50 MHz and 90 MHz, respectively. As shown in Figure 9, the real PD signal could not be observed after mixing narrowband noise.

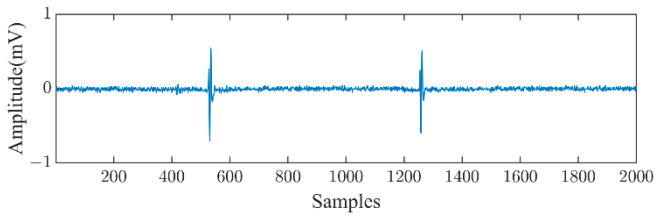

Figure 8. Real PD signal.

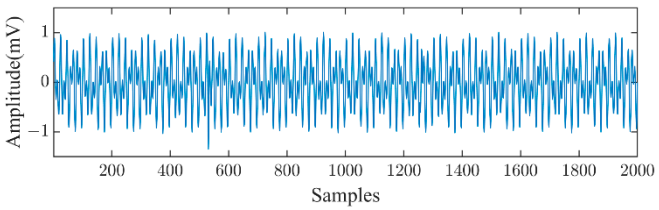

Figure 9. Real PD signal after mixing noise.

Figure 10 shows the denoising results for the real PD signal by FPA-VMD-SG, EMD-WT, and ASVD. In the FPA-VMD-SG method, the final optimization parameters of VMD were $K = 4$ and $\alpha = 6309.9435$. The polynomial order of the SG filter was 2 and the frame length was 201. The coefficient c of threshold denoising was 2.2. For WT parameter settings in the EMD-WT, the decomposition level was 7, the wavelet was 'db4', the threshold was 'rigrsure', and the denoising method was soft threshold denoising.

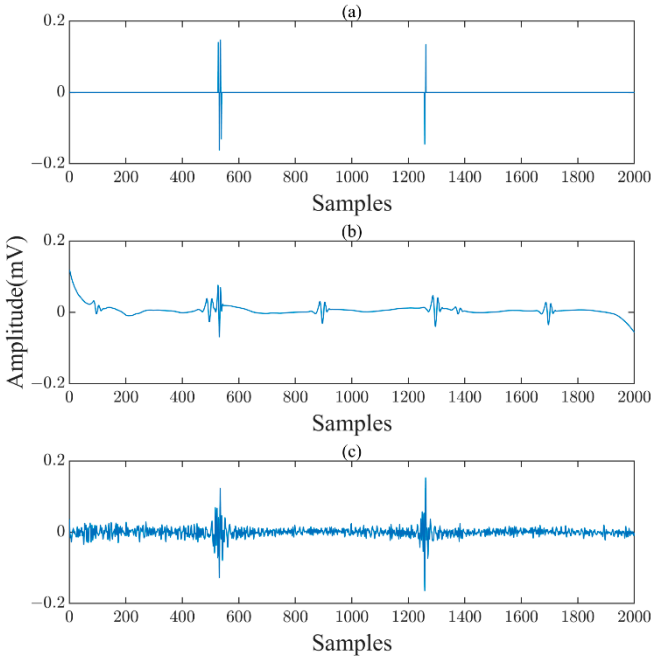

Figure 10. The denoising results of real PD by different methods: (**a**) FPA-VMD-SG; (**b**) EMD-WT; (**c**) ASVD.

Since the original PD signal without noise could not be obtained and the denoising performance could not be evaluated by *SNR*, *NCC*, or *RMSE*, the noise reduction ratio (*NRR*) was introduced to evaluate the denoising performance [12]. The *NRR* value was higher and the denoising performance was better. It was defined as:

$$NRR = 10 * \left(\log_{10} \sigma_1^2 - \log_{10} \sigma_2^2 \right) \tag{20}$$

where σ_1 and σ_2 are the standard deviations of the real PD signal and denoised PD signal, respectively.

Comparing the denoising results of the three methods, it can be seen that the FPA-VMD-SG could effectively retain the PD signal and remove white noise and narrowband noise. The EMD-WT had a few white noise residues and wrongly removed the PD signal. The ASVD could effectively remove narrowband noise, but the removal of white noise was slightly insufficient. The *NRR* values of the three denoising methods are shown in Table 3. Among the three methods, the *NRR* value of the FPA-VMD-SG was the highest at 14.5893, indicating that the proposed denoising method had the best performance in suppressing noise and retaining the PD signal.

Table 3. *NRR* values of three denoising methods.

	EMD-WT	**ASVD**	**FPA-VMD-SG**
NRR	9.4793	10.0246	14.5893

5. Conclusions

In this paper, a novel denoising method by integrating the VMD, FPA, and SG filter was proposed to realize the suppression of white noise and narrowband noise inhe PD signal. According to the denoising results of simulated and real PD signals, the following conclusions can be drawn:

(1) Based on the MME, the appropriate parameters K. and α of VMD could be found by FPA.
(2) The VMD had excellent anti-modal mixing characteristics, which could decompose the PD noise signal properly.
(3) The SG filter could effectively remove the noise in the noise component and retain the PD signal.
(4) The FPA-VMD-SG method could effectively suppress white noise and narrowband noise in the PD signal.

Author Contributions: Conceptualization, J.Y. and X.Z.; Data curation, J.Y.; Formal analysis, X.Z.; Funding acquisition, J.Y. and K.Y.; Investigation, J.Y.; Methodology, J.Y. and K.Y.; Project administration, X.Z.; Resources, X.Z.; Software, J.Y., K.Y. and Z.W.; Supervision, X.Z.; Validation, J.Y., K.Y. and Z.W.; Visualization, J.Y. and K.Y.; Writing—original draft, J.Y.; Writing—review & editing, K.Y. and Z.W. All authors have read and agreed to the published version of the manuscript.

Funding: This research was funded by the Postgraduate Research and Practice Innovation Program of Jiangsu Province, grant number KYCX21_0869.

Data Availability Statement: The data used in this study is available from the authors upon requests.

Conflicts of Interest: The authors declare no conflict of interest.

References

1. Zhang, Z.; Lei, J.; Chen, W.; Yang, T.; Song, Y.; Wu, K.; Liu, F. Oil-paper insulation partial discharge ultrasonic multifrequency sensing array based on fibre-optic Fabry—Perot sensor. *High Volt.* **2022**, *7*, 325–335. [CrossRef]
2. Song, H.; Dai, J.; Sheng, G.; Jiang, X. GIS partial discharge pattern recognition via deep convolutional neural network under complex data source. *IEEE Trans. Dielectr. Electr. Insul.* **2018**, *25*, 678–685. [CrossRef]
3. Firuzi, K.; Vakilian, M.; Phung, B.T.; Blackburn, T.R. Partial discharges pattern recognition of transformer defect model by LBP & HOG features. *IEEE Trans. Power Del.* **2019**, *34*, 542–550.
4. Luo, L.; Han, B.; Chen, J.; Sheng, G.; Jiang, X. Partial discharge detection and recognition in random matrix theory paradigm. *IEEE Access* **2016**, *5*, 8205–8213. [CrossRef]
5. Zhong, J.; Bi, X.; Shu, Q.; Chen, M.; Zhou, D.; Zhang, D. Partial dscharge signal denoising based on singular value decomposition and empirical wavelet transform. *IEEE Trans. Instrum. Meas.* **2020**, *69*, 8866–8873. [CrossRef]
6. Zhou, S.; Tang, J.; Pan, C.; Luo, Y.; Yan, K. Partial discharge signal denoising based on wavelet pair and block thresholding. *IEEE Access* **2020**, *8*, 119688–119696. [CrossRef]
7. Tang, J.; Zhou, S.; Pan, C. A denoising algorithm for partial discharge measurement based on the combination of wavelet threshold and total variation theory. *IEEE Trans. Instrum. Meas.* **2020**, *69*, 3428–3441. [CrossRef]
8. Chen, X.; Yang, Y. Analysis of the partial discharge of ultrasonic signals in large motor based on Hilbert-Huang transform. *Appl. Acoust.* **2018**, *131*, 165–173. [CrossRef]
9. Jin, T.; Li, Q.; Mohamed, M.A. A novel adaptive EEMD method for switchgear partial discharge signal denoising. *IEEE Access* **2019**, *7*, 58139–58147. [CrossRef]
10. Zhang, S.; Liu, H.; Hu, M.; Jiang, A.; Zhang, L.; Xu, F.; Hao, G. An adaptive CEEMDAN thresholding denoising method optimized by nonlocal means algorithm. *IEEE Trans. Instrum. Meas.* **2020**, *69*, 6891–6903. [CrossRef]
11. Zhou, K.; Li, M.; Li, Y.; Xie, M.; Huang, Y. An improved denoising method for partial discharge signals contaminated by white noise based on adaptive short-time singular value decomposition. *Energies* **2019**, *12*, 3465. [CrossRef]
12. Yang, X.; Huang, H.; Shu, Q.; Zhang, D.; Chen, B. Partial discharge signal extraction method based on EDSSV and low rank RBF neural network. *IEEE Access* **2021**, *9*, 9744–9752. [CrossRef]
13. Dhandapani, R.; Mitiche, I.; McMeekin, S.; Mallela, V.S.; Morison, G. Enhanced partial discharge signal denoising using dispersion entropy optimized variational mode decomposition. *Entropy* **2021**, *23*, 1567. [CrossRef]
14. Long, J.; Wang, X.; Dai, D.; Tian, M.; Zhu, G.; Zhang, J. Denoising of UHF PD signals based on optimised VMD and wavelet transform. *IET. Sci. Meas. Technol.* **2017**, *11*, 753–760. [CrossRef]
15. Wu, Z.; Huang, N.E. Ensemble empirical mode decomposition: A noise-assisted data analysis method. *Adv. Adapt. Data Anal.* **2009**, *1*, 1–41. [CrossRef]

16. Yeh, J.-R.; Shieh, J.-S.; Huang, N.E. Complementary ensemble empirical mode decomposition: A novel noise enhanced data analysis method. *Adv. Adapt. Data Anal.* **2010**, *2*, 135–156. [CrossRef]
17. Torres, M.E.; Colominas, M.A.; Schlotthauer, G.; Flandrin, P. A complete ensemble empirical mode decomposition with adaptive noise. In Proceedings of the IEEE International Conference on Acoustics, Speech and Signal Processing (ICASSP), Prague, Czech Republic, 22–27 May 2011; pp. 4144–4147.
18. Ashtiani, M.B.; Shahrtash, S.M. Partial discharge de-noising employing adaptive singular value decomposition. *IEEE Trans. Dielectr. Electr. Insul.* **2014**, *21*, 775–782. [CrossRef]
19. Dragomiretskiy, K.; Zosso, D. Variational mode decomposition. *IEEE Trans. Signal Process.* **2014**, *62*, 531–544. [CrossRef]
20. Shen, S.; Xu, J. Trajectory tracking active disturbance rejection control of the unmanned helicopter and its parameters tuning. *IEEE Access* **2021**, *9*, 56773–56785. [CrossRef]
21. Yang, X.-S. Flower pollination algorithm for global optimization. In *International Conference on Unconventional Computing and Natural Computation*; Springer: Berlin/Heidelberg, Germany, 2012; pp. 240–249.
22. Wang, M.; Wang, W.; Zeng, J.; Zhang, Y. An integrated method based on sparrow search algorithm improved variational mode decomposition and support vector machine for fault diagnosis of rolling bearing. *J. Vib. Eng. Technol.* **2022**, 1–12. [CrossRef]
23. Schafer, R.W. What is a Savitzky-Golay filter? [Lecture Notes]. *IEEE Signal Process. Mag.* **2011**, *28*, 111–117. [CrossRef]
24. Savitzky, A.; Golay, M.J. Smoothing and differentiation of data by simplified least squares procedures. *Anal. Chem.* **1964**, *36*, 1627–1639. [CrossRef]
25. Chen, L.; Zhang, W.; Ye, H. Accurate workload prediction for edge data centers: Savitzky-Golay filter, CNN and BiLSTM with attention mechanism. *Appl. Intell.* **2022**, *52*, 13027–13042. [CrossRef]
26. Lin, M.-Y.; Tai, C.-C.; Tang, Y.-W.; Su, C.-C. Partial discharge signal extracting using the empirical mode decomposition with wavelet transform. In Proceedings of the 7th Asia-Pacific International Conference on Lightning, Chengdu, China, 1–4 November 2011; pp. 420–424.
27. Thuc, V.C.; Lee, H.S. Partial Discharge (PD) Signal Detection and Isolation on High Voltage Equipment Using Improved Complete EEMD Method. *Energies* **2022**, *15*, 5819. [CrossRef]
28. Smith, T.; Mahmoodi, D. ELEC6089-PD-Analysis. Available online: https://github.com/TheSmiff/ELEC6089-PD-Analysis (accessed on 6 March 2022).